Capturing near wall effects when applying the Algebraic Structured Based Model

By J. P. O'Sullivan†, R. Pecnik‡ AND G. Iaccarino¶

Two new near-wall treatments have been implemented for use with the algebraic structure based turbulence model (ASBM) enabling its application to more complex flows. The first extended the standard wall blocking model to take account for multiple walls. The results show that the new wall blocking model enables the ASBM to correctly predict the turbulent state of flows near to internal corners. Second, a new wall function for the shear component of the Reynolds stress tensor has been developed. The wall function performed well when compared to other simulations and experimental data and produced results very similar to those obtained using tabulated wall functions. A rough wall form of the wall function is also presented, enabling the simulation of high Reynolds number industrial and environmental flows using the ASBM.

1. Introduction

Despite the rapid advancement of computational power and improvements in numerical techniques, solving many environmental and industrial flows remains beyond the capabilities of large-eddy simulation (LES) and direct numerical simulation (DNS). Instead the Reynolds-averaged Navier-Stokes (RANS) approach is likely continue to be the most popular method for solving these types of flows over the coming years (Hanjalic 2005). However, turbulence modeling within the RANS approach remains a significant challenge. The limitations of eddy-viscosity models have been highlighted by many researchers as has the inability of standard turbulence models to reproduce turbulent anisotropy.

Common Reynolds stress models only provide information about the magnitude of each of the components (referred to as componentality). Since the early 1990's Reynolds and coworkers (see Kassinos *et al.* (2006) and the references therein) have argued that information about the turbulence *structure* is also required to accurately characterize the turbulence field. They introduced the concepts of *structure dimensionality* and *structure circulicity* to provide this information. The dimensionality tensor gives the level of two-dimensionality of the turbulence while the circulicity describes the large-scale structure of the vorticity field (Kassinos *et al.* 2001). The important distinction between the componentality and dimensionality of turbulence is described clearly by Kassinos & Reynolds (1995) using the concept of three basic, idealized eddies: jettal, vortical and helical, and by considering two important examples of rapid deformation.

The representation of turbulence in terms of its structure tensors opened the way for a whole family of structure based models. The algebraic structure based model (ASBM) belongs to this family and detailed descriptions of the model and its development can be found in Kassinos & Reynolds (1995); Kassinos *et al.* (2000, 2001, 2006).

The ASBM has now been successfully applied to a number of test cases that include

† University of Auckland, New Zealand
‡ Delft University of Technology, The Netherlands
¶ Stanford, California, USA

effects such as separation and rotating flows (Kassinos *et al.* 2006; Radhakrishnan *et al.* 2008; O'Sullivan *et al.* 2010). In order to extend the range of its applicability, more complex and realistic test cases must be attempted. In this work two new test cases were investigated and extensions to the ASBM are proposed. The first is the three-dimensional flow inside a square duct. This is an important test case as it is representative of internal flows and introduces the additional complexity of internal corners. The standard ASBM uses a wall-blocking approach to capture the flow effects in the near-wall region. This work extends the wall-blocking approach to include the effects of corners in such a way that the true state of the turbulence is accurately captured in the near-wall region.

The second test case addresses a different issue. For the ASBM to be applied to environmental flows such as wind flow over complex terrain, an appropriate near-wall treatment must be developed that is compatible with the model. Flows of this nature feature very high Reynolds numbers and three-dimensional effects and surface roughness combine to prevent the use of wall-resolved grids. This work presents wall functions which have been developed for use with the ASBM to enable the simulation of large-scale environmental flows. They are tested on a representative flow and the results are compared with those from a fully resolved simulation and a simulation using tabulated wall functions.

2. Wall blocking

In the near wall-region the ASBM uses wall blocking to model the changes in the state of the turbulence that are observed in the DNS data (Reynolds *et al.* 2000). The approach is to include a blockage tensor B_{ij} that acts upon the eddy-axis tensor a_{ij} to re-orient the eddies to be parallel to the wall as they approach it, using

$$a_{ij} = H_{ik} H_{jl} a^h_{kl} \ , \tag{2.1}$$

where a^h_{ij} is the homogeneous eddy-axis tensor and H_{ij} is the partial-projection operator given by:

$$H_{ij} = \frac{1}{D_a} \left(\delta_{ij} - B_{ij} \right) , \quad D_a^2 = 1 - (2 - B_{kk}) a^h_{mn} B_{mn} \ . \tag{2.2}$$

The blockage tensor is defined as follows:

$$B_{ij} = \frac{\frac{\partial \phi}{\partial x_i} \frac{\partial \phi}{\partial x_j}}{\frac{\partial \phi}{\partial x_k} \frac{\partial \phi}{\partial x_k}} \ , \tag{2.3}$$

where ϕ is the solution of the modified Helmholtz equation:

$$L^2 \frac{\partial^2 \phi}{\partial x_k \partial x_k} = \phi \ , \quad L = C_L \max \left(\frac{k^{3/2}}{\varepsilon}, C_\nu \sqrt[4]{\frac{\nu^3}{\varepsilon}} \right) . \tag{2.4}$$

The constants in Eq. (2.4) are $C_L = 0.80$ and $C_\nu = 0.17$ following Radhakrishnan *et al.* (2008). For boundary conditions $\phi = 1$ at solid walls and $\partial \phi / \partial x_n = 0$ where x_n is the wall-normal direction.

This approach is based on the elliptic relaxation model proposed by Durbin (1991) but uses only a single parameter, ϕ, to calculate the influence of the wall. In the presence of multiple walls, such as at a corner, each wall must affect the flow and will play a part in determining the state of the turbulence. To represent this effect, the parameter is extended from a scalar quantity to a vector quantity ϕ_i, which gives rise to the terminology "scalar wall blocking" and "vector wall blocking."

2.1. *Vector wall blocking*

Applying vector wall blocking requires that Eq. (2.4) is solved in each of the coordinate directions with the boundary conditions applied only for that direction. Thus at a wall normal to the x-direction the boundary conditions applied are $\phi_x = 1$ and $\partial\phi_y/\partial x = \partial\phi_z/\partial x = 0$.

Once ϕ_i has been calculated, blockage tensors can be calculated using Eq. (2.3) for each direction B^x_{ij}, B^y_{ij} and B^z_{ij}. The eddy-axis tensor is then calculated by applying each of the partial-projection operators sequentially. This can be expressed as follows:

$$\begin{aligned} a^x_{ij} &= (\delta_{ik} - B^x_{ik})(\delta_{jl} - B^x_{jl})a^h_{kl} \ ; \\ a^y_{ij} &= (\delta_{ik} - B^y_{ik})(\delta_{jl} - B^y_{jl})a^x_{kl} \ ; \\ a^z_{ij} &= (\delta_{ik} - B^z_{ik})(\delta_{jl} - B^z_{jl})a^y_{kl} \ ; \\ a_{ij} &= a^z_{ij}/a^z_{kk} \ . \end{aligned} \tag{2.5}$$

It is important to note that the partial-projection operators are non-commutative and the order in which they are applied in Eq. (2.5) is arbitrary. Therefore, to represent their cumulative effect independently of the frame of reference, a_{ij} is calculated for each permutation of partial-projection operators and an average obtained.

2.2. *Results*

The results presented in this section were obtained using the data from a DNS of a square duct flow carried out by Pecnik *et al.* (2012, private communication). The velocity field of the DNS was used as the input to the ASBM and the resulting turbulence field was calculated using three different wall blocking approaches: no wall blocking, scalar wall blocking and vector wall blocking. The value of the viscosity used in the DNS was calculated to achieve a Reynolds number based on the friction velocity $Re_\tau = 360$ which corresponded to a bulk $Re \approx 5400$.

Barycentric maps are used to present the results as these provide a non-distorted visual representation of anisotropy in turbulent quantities (Banerjee *et al.* 2007). The barycentric maps use the eigenvalues of the Reynolds stress tensor to calculate a linear representation of its anisotropy invariants. This makes it possible to quantify any point in the turbulent field in terms of the one-, two- and three-component limiting states.

The barycentric map of the DNS turbulence field in Figure 1 (a) shows that by moving from the center of the duct to the center of the wall, the turbulence changes from a near isotropic state, towards a one-component state and then finally at the wall itself tends rapidly towards the two-component limit. The results for the case in which no wall blocking was applied show the poorest agreement with the DNS results, which demonstrates the need for wall blocking. In the no wall blocking case the turbulence also changes towards the one-component limit but traversing a different trajectory. As the wall is approached and no blocking occurs, the ASBM tends push the turbulence back towards an isotropic three-component state. As expected the scalar wall blocking and the vector wall blocking produce the same results as the trajectory is far from the corners. Both formalisms agree very well with the DNS results, as a similar trajectory is followed towards the one-component limit before the turbulence turns towards the two-component limit at the wall.

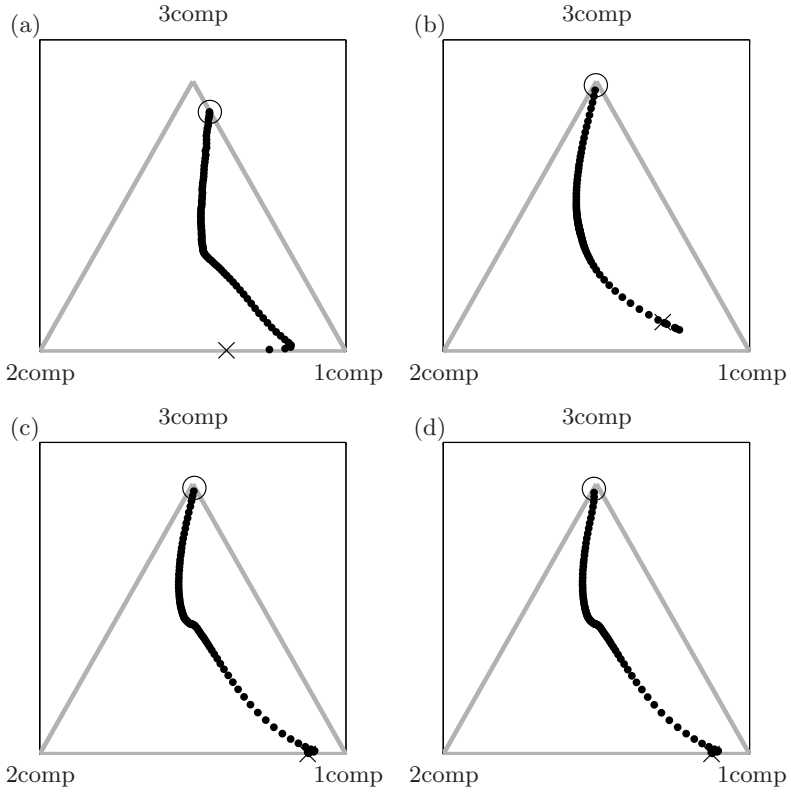

FIGURE 1. Barycentric maps for the trajectory from the center of the duct to the center of the bottom wall comparing (a) DNS results (b) no wall blocking (c) scalar wall blocking and (d) vector wall blocking. Start of the trajectory indicated with (○) and the end with (×).

In Figure 2, the importance of the vector wall blocking can be seen. The results from the DNS turbulence field show the trajectory in the barycentric map remains close to the edge of the map as it approaches and finally arrives at the one-component limit. The ASBM without wall blocking is not able to capture this behavior correctly and the incorrect trajectory is followed before the turbulence tends back towards a three-component state as the corner is approached. Using scalar blocking also fails to predict the state of the turbulence correctly. Moving towards the corner the scalar wall blocking has little effect and the trajectory is similar to the no wall blocking case. Arriving at the corner, the scalar wall blocking tends towards the one-component state before incorrectly turning towards the two-component limit. This occurs because the scalar wall blocking effectively models the corner as a single wall at 45° and incorrectly aligns the eddy-axis. The vector wall blocking correctly ensures that the turbulence remains close to the edge of the barycentric map before arriving at the one-component state. By applying the partial-projection operator to the eddy-axis tensor for one wall and then the other, it is essentially reduced to a jettal component aligned along the corner of the duct.

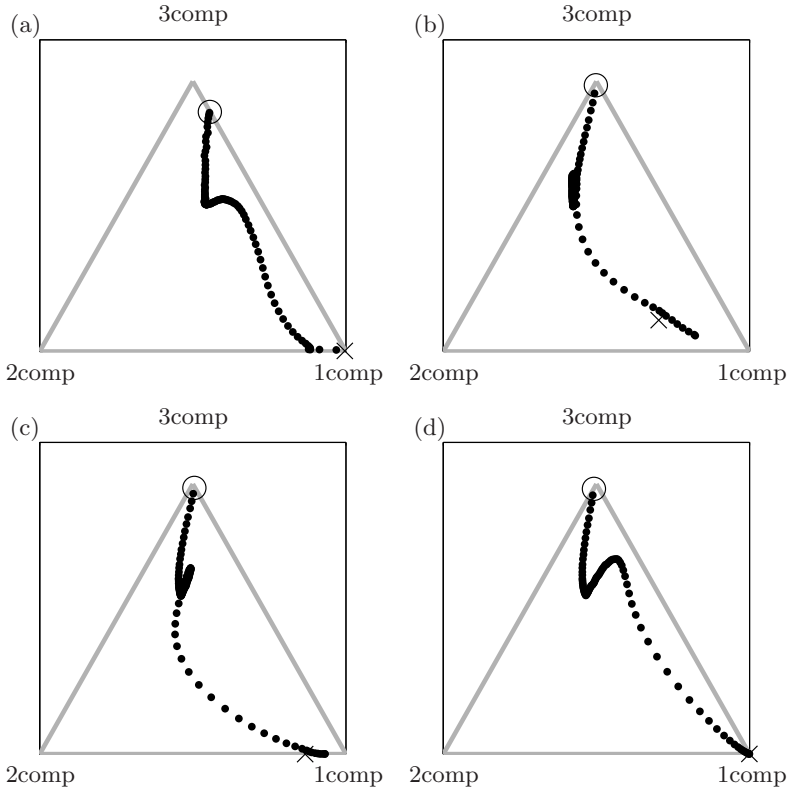

FIGURE 2. Barycentric maps for the trajectory from the center of the duct to the bottom left corner comparing (a) DNS results (b) no wall blocking (c) scalar wall blocking and (d) vector wall blocking. Start of the trajectory indicated with (∘) and the end with (×).

3. Wall functions

Wall functions apply boundary conditions at some distance from the wall, which removes the requirement to solve the governing equations all the way to the wall. This has two important benefits in simulations of large-scale, industrial and environmental flows. First, it significantly reduces the computational resource required by allowing the use of a much coarser grid near the wall. Second, by applying the boundary conditions at some point away from the wall, the exact geometry of the wall does not need to be fully resolved. This allows the complex geometries caused by terrain effects, vegetation, etc., to be modeled by including an equivalent roughness in the wall functions. While standard wall functions can be used with the more common turbulence closures, using the ASBM requires the development of new wall functions.

3.1. *The standard wall functions*

The standard wall function model presented by Launder & Spalding (1974) with Wilcox's (1998) estimate of the friction velocity u_τ can be summarized as:

$$u^+ = \frac{1}{\kappa}\ln\left(y^+\right) + B \ , \quad u^+ = \frac{u}{u_\tau} \ , \quad y^+ = \frac{u_\tau y}{\nu} \ , \quad u_\tau = C_\mu^{1/4} k_1^{1/2} \ . \tag{3.1}$$

In Eq. (3.1) u is the tangential velocity, y is the wall-normal distance and the + indicates their non-dimensional values. Note that to avoid problems caused by $y^+ \to 0$ at separation and reattachment points, a no-slip boundary condition is applied if $y^+ < 5$.

In general, the log law approximations are not applied directly to the velocity but instead are used to adjust the eddy viscosity ν_T at the wall. Similarly, the turbulent kinetic energy is not defined by the wall function in the near-wall cell, but instead the wall shear stress is approximated using the log law and this is included in the production term in the turbulent kinetic energy equation.

$$\nu_T = \nu \left(\frac{y^+}{u^+} - 1 \right) \ , \quad \mathcal{P}_1 = \tau_w \left. \frac{\partial u}{\partial y} \right|_1 , \text{ with: } \quad \tau_w = C_\mu^{1/4} k_1^{1/2} \frac{u_1}{u^+} \ . \tag{3.2}$$

The effects of roughness are easily introduced into the standard wall functions by adjusting the non-dimensional wall velocity and wall shear stress accordingly:

$$u^+_{rough} = \frac{1}{\kappa} \ln \left(\frac{y^+}{K_s^+} \right) + B_{rough} \ , \quad \tau_{wrough} = C_\mu^{1/4} k_1^{1/2} \frac{u_1}{u^+_{rough}}, \tag{3.3}$$

where K_s^+ is the non-dimensional equivalent grain-of-sand roughness height which is determined by the surface. B_{rough} is the rough wall log law constant and for the present work a value of 8.5 was used (Pope 2000).

3.2. *An analytic wall function for* $\overline{u'v'}$

When the ASBM is used for estimating the components of the Reynolds stress tensor, the domain must again be resolved all the way to the viscous sublayer. Applying the ASBM closure on a coarse grid gives poor results for the mean flow and all the variables in the near-wall cell. In particular, investigations have shown it overestimates the shear component of the Reynolds stress tensor in the near-wall cell, which leads to large overestimations in the mean velocity and subsequently all of the other variables. To correct this, the shear component of the Reynolds stress tensor in the near-wall cell is estimated by assuming that locally the flow approximates turbulent Couette flow. In this situation the total shear stress can be calculated by:

$$\tau = \rho \, \nu \frac{\partial u}{\partial y} - \rho \, \overline{u'v'} \ . \tag{3.4}$$

This equation can be solved to give an expression for τ dependent only on τ_w, the wall distance y and the boundary-layer thickness δ (Pope 2000):

$$\tau(y) = \tau_w \left(1 - \frac{y}{\delta} \right) \ . \tag{3.5}$$

By combining Eqs. (3.4) and (3.5), an expression for the shear component of the Reynolds stress tensor can be obtained and applied at the near-wall cell:

$$\overline{u'v'}_1 = \nu \left. \frac{\partial u}{\partial y} \right|_1 - \frac{\tau_w}{\rho} \left(1 - \frac{y_1}{\delta} \right) \ . \tag{3.6}$$

Eq. (3.2) can be used to calculate τ_w making the wall function consistent with those used for the other variables, increasing its robustness and providing a simple mechanism for introducing roughness. To estimate the local boundary-layer thickness, it is assumed that the gradient of $\overline{u} \to 0$ as $y \to \delta$. From this δ can be approximated as the point at

which the gradient of $\overline{u}$ drops below a certain value β giving:

$$\delta = \frac{u_\tau}{\kappa\beta} \ . \tag{3.7}$$

Studies of channel flows of known boundary-layer height found that simulation results were not sensitive to the choice of β (O'Sullivan 2012) and that $\beta = 0.5$ gave good estimates of δ. This value was used for all the simulations.

Once the shear component of the Reynolds stress tensor has been calculated using Eq. (3.6) it is important to apply it correctly. This requires rotating the Reynolds stress tensor so that it is aligned with the wall-normal direction and the tangential velocity, correcting the shear component in this orientation, then rotating the corrected tensor back into the grid aligned coordinates. At each point care must be taken to ensure that the components of $\overline{u_i' u_j'}$ maintain the correct sign, especially in areas of complex flow such as separation and re-attachment points. Note that following Pope (2000) there is also a small adjustment in the calculation of τ in the rough wall case:

$$\tau(z)_{rough} = \tau_{wrough} \left(1 - \frac{z - z_0}{\delta} \right) \ , \tag{3.8}$$

where the offset z_0 is the aerodynamic roughness height.

3.3. *Tabulated wall functions*

Tabulated wall functions provide an alternative to the analytic model presented above and remove the need to estimate u_τ using Eq. (3.1). Kalitzin *et al.* (2005) showed that by calculating a local Reynolds number in the near-wall cell, the non-dimensional values of each of the solution variables can be interpolated from tabulated data. The value of y^+ can be interpolated from the same table and by using the interpolated value of u^+ the value of u_τ can be calculated. Using y^+, u_τ and ν the variables can each be dimensionalized to give their value in the near-wall cell. To create the tabulated data a finely resolved simulation of a channel flow must be performed. Fortunately this can be carried out as a pre-processing task and need only be performed once. One of the advantages of the tabulated wall functions is that they are valid for all y^+ and so no special treatment is required near separation points. However unlike the analytical wall functions additional parameters such as roughness require new tabulated data and new channel simulation would be required for each roughness length.

3.4. *Results*

The wall functions were tested using a high Reynolds number flow over a two-dimensional bump investigated as part of a NASA research project (Viken *et al.* 2003). The flow has a large separated region which provided a challenging test for the wall functions and there is a good set of experimental data for comparison. The wall-resolved grid fulfilled the standard requirement of $y_1^+ < 1.0$ and had 108 cells in the wall-normal direction. The same wall-function grid was used for both types of wall functions and had 39 cells in the wall-normal direction and $y_1^+ \approx 20$.

Comparing plots (a) and (b) in Figure 3 it can be seen that in the wall-resolved simulation the ASBM captures the separated region quite well but overestimates the reattachment point. This behavior has been observed previously (O'Sullivan *et al.* 2010) and is accompanied by an underestimation of the Reynolds stresses in the separated region. Plots (c) and (d) show that not only do both the analytic wall functions and the tabulated wall functions perform very well, they more accurately estimate the separated

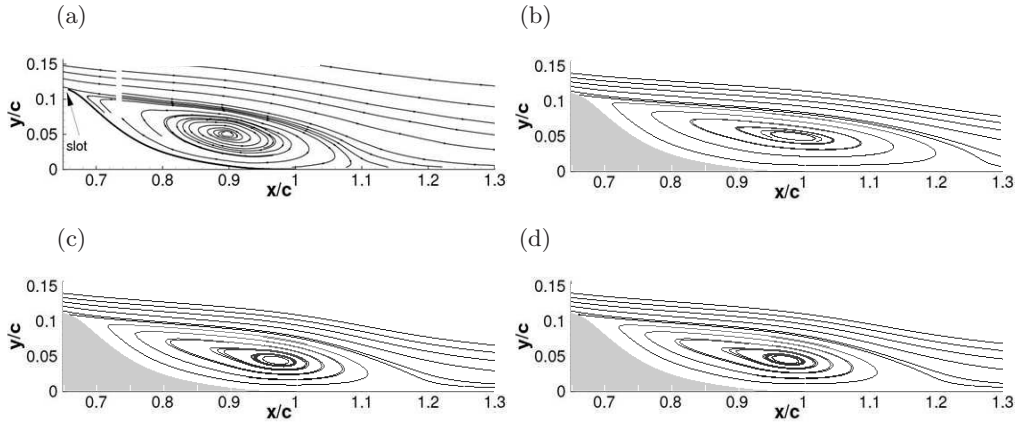

FIGURE 3. Comparison of velocity streamlines for (a) experimental results (Viken *et al.* 2003) and simulations using (b) a wall-resolved grid, (c) analytic wall functions and (d) tabulated wall functions.

region than the wall-resolved simulation. In all three simulations, the results are very similar until $x/c \approx 1$ where the center of the recirculation is predicted. However both wall-function simulations predict a shorter recovery region and hence a smaller separated region. While it is disconcerting that *inherently less accurate* models can provide better estimates, it can in fact be instructive in identifying issues with the ASBM.

The plots in Figure 4 give a more in depth view of the results in the cells adjacent to the wall in the wall-function simulations and at the same wall-normal distance in the wall-resolved simulation. The turbulent kinetic energy estimated by each simulation is plotted in (b). This shows that adjacent to the wall all three simulations estimate similar levels of k until the center of the recirculation is reached at $x/c \approx 1$. Beyond this point the wall-functions predict that k falls and the tabulated wall-function estimates it approaches 0 at the separation point. However in the wall-resolved simulation at the same wall-normal distance, the value of k continues to rise before falling only slightly at the reattachment point. This indicates that in regions of reversed flow and high velocity gradients the ASBM overestimates the production of k. The wall functions alleviate this by applying an approximate wall treatment in this region. Figure 5 reveals another possible contributing factor. It shows the $\overline{u'v'}$ profiles for each simulation and the experimental data immediately adjacent to the wall. All of the simulations erroneously predict positive shear stress at the wall at $x/c = 1$. However by $x/c = 1.1$, this error is almost zero for the wall-function simulations whereas it remains in the wall-resolved simulation. At $x/c = 1.2$, a small positive value is still present at the wall in the wall-resolved simulation. This erroneous positive shear acts to accelerate the flow in the streamwise direction and could play a role in extending the separated region.

The results in Figures 3 - 5 demonstrate how similar the results obtained by the two different wall-function approaches are, hence showing that the analytic functions presented in Section 3 provide accurate models. One possible advantage of the tabulated wall functions is highlighted in plot (c) of Figure 4. Here it can be seen that at the separation point, as the velocity drops to zero, $\overline{u'v'}$ remains smooth in the tabulated wall function simulation where it does not in the analytic wall function simulation. For this test case this effect had no impact on the overall flow but it may not always be the case.

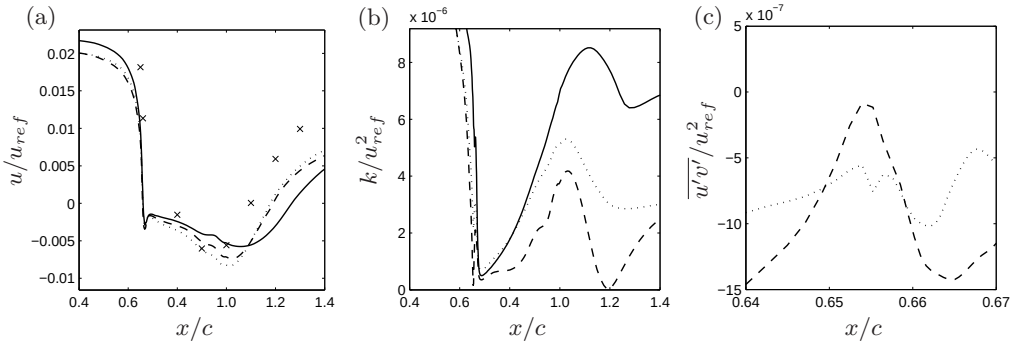

FIGURE 4. Plots comparing (a) streamwise velocity (b) turbulent kinetic energy and (c) Reynolds shear stress obtained at constant wall-normal distance for simulations using a wall-resolved grid (—), analytic wall functions (...) and tabulated wall functions(- -). Experimental results (Viken *et al.* 2003) also shown (×).

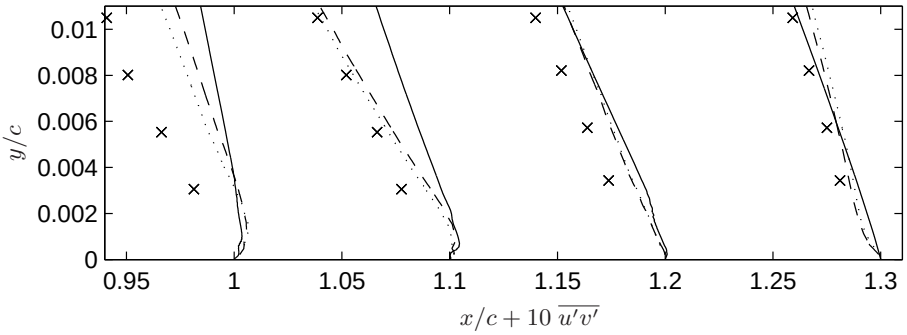

FIGURE 5. Plot comparing Reynolds shear stress for simulations using a wall-resolved grid (—), analytic wall functions (...) and tabulated wall functions(- -). Experimental results (Viken *et al.* 2003) also shown (×).

4. Conclusions

Two new near-wall treatments have been implemented for use with the ASBM. The first extended the standard wall blocking model used in the ASBM to take account for multiple walls. The results show that the new wall blocking model enables the ASBM to correctly predict the turbulent state of flows near to internal corners. Second a new wall function for the shear component of the Reynolds stress tensor has been developed. The new wall function is consistent with standard wall functions and a rough wall implementation has also been presented. The wall function performed well when compared to other simulations and experimental data and produced results very similar to those obtained using tabulated wall functions. For the present test case both wall-function simulations produced more accurate results than the wall-resolved simulation. This unusual result occurs because the approximate nature of wall functions reduces errors in the current implementation of the ASBM that occur near the wall in the separated region. Finally, while the tabulated wall functions offer more accuracy as $y^+ \to 0$, the new wall function is simple to implement and can be used for varying roughness without the need for numerous preliminary simulations. The new wall function can be used with any turbulence closure solving for the full Reynolds stress tensor.

Acknowledgments

Many thanks go to Stavros Kassinos and his team, Ik Jang and Paul Durbin for the interesting and helpful discussions. JPO and RP gratefully acknowledge support from the Center for Turbulence Research at Stanford University, the University of Auckland and Delft University of Technology.

REFERENCES

Banerjee, S., Krahl, R., Durst, F. & Zenger, C. 2007 Presentation of anisotropy properties of turbulence, invariants versus eigenvalue approaches. *Journal of Turbulence* **8** (32), 1–27.

Durbin, P. A. 1991 Near-wall turbulence closure modeling without damping functions. *Theoretical and Computational Fluid Dynamics* **3** (1), 1–13.

Hanjalic, K. 2005 Will RANS survive LES? a view of perspectives. *J. of Fluids Engineering* **127** (5), 831–839.

Kalitzin, G., Medic, G., Iaccarino, G. & Durbin, P. 2005 Near-wall behavior of rans turbulence models and implications for wall functions. *J. of Computational Physics* **204** (1), 265–291.

Kassinos, S. C., Langer, C. A., Haire, S. L. & Reynolds, W. C. 2000 Structure-based turbulence modeling for wall-bounded flows. *International Journal of Heat and Fluid Flow* **21** (5), 599–605.

Kassinos, S. C., Langer, C. A., Kalitzin, G. & Iaccarino, G. 2006 A simplified structure-based model using standard turbulence scale equations: computation of rotating wall-bounded flows. *International Journal of Heat and Fluid Flow* **27** (4), 653–660.

Kassinos, S. C. & Reynolds, W. C. 1995 A structure-based model for the rapid distortion of homogeneous turbulence. *Tech. Rep.* TF-61. Stanford University.

Kassinos, S. C., Reynolds, W. C. & Rogers, M. 2001 One-point turbulence structure tensors. *Journal of Fluid Mechanics* **428**, 213–248.

Launder, B. E. & Spalding, D. B. 1974 The numerical computation of turbulent flows. *Computer Methods in Applied Mechanics and Engineering* **3** (2), 269–289.

O'Sullivan, J. P. 2012 Modelling wind flow over complex terrain. PhD thesis, University of Auckland.

O'Sullivan, J. P., Pecnik, R. & Iaccarino, G. 2010 Investigating turbulence in wind flow over complex terrain. In *Proceedings of the Summer Program 2010*, pp. 129–139. Stanford University.

Pope, S. B. 2000 *Turbulent flows*. New York: Cambridge University Press.

Radhakrishnan, H., Pecnik, R., Iaccarino, G. & Kassinos, S. C. 2008 Computation of separated turbulent flows using the asbm model. In *Proceedings of the Summer Program 2008*, pp. 365–376. Stanford University.

Reynolds, W. C., Kassinos, S. C., Langer, C. A. & Haire, S. L. 2000 New directions in turbulence modeling. In *Third International Symposium on Turbulence, Heat and Mass Transfer*. Nagoya, Japan.

Viken, S., Vatsa, V. & Rumsey, C. 2003 Flow control analysis of the hump model with rans tools. *Tech. Rep.* AIAA 2003-0218.

Wilcox, D. C. 1998 *Turbulence modeling for CFD*, 2nd edn. La Canada: DWC Industries.